Skeletal Radiology (2022) 51:1731–1741
https://doi.org/10.1007/s00256-022-04032-6

REVIEW ARTICLE

Utility of dual energy computed tomography in the evaluation of infiltrative skeletal lesions and metastasis: a literature review

Martin Toby Tan[1] · **Thomas Bernard Lloyd**[1]

Received: 26 December 2021 / Revised: 7 March 2022 / Accepted: 7 March 2022 / Published online: 16 March 2022

Abstract

Computed tomography (CT) is routinely used to diagnose and evaluate metastatic lesions in oncology. CT alone suffers from lack of sensitivity, especially for skeletal lesions in the bone marrow and lesions that have similar attenuation profiles to surrounding bone. Magnetic resonance imaging and nuclear medicine imaging remain the gold standard in evaluating skeletal lesions. However, compared to CT, these modalities are not as widely available or suitable for all patients. Dual energy computed tomography (DECT) exploits variations in linear attenuation coefficient of materials at different photon energy levels to reconstruct images based on material composition. DECT in musculoskeletal imaging is used in the imaging of crystal arthropathy and detecting subtle fractures, but it is not broadly utilized in evaluating infiltrative skeletal lesions. Malignant skeletal lesions have different tissue and molecular compositions compared to normal bone. DECT may exploit these physical differences to delineate infiltrative skeletal lesions from surrounding bone better than conventional monoenergetic CT. Studies so far have examined the utility of DECT in evaluating skeletal metastases, multiple myeloma lesions, pathologic fractures, and performing image-guided biopsies with promising results. These studies were mostly retrospective analyses and case reports containing small samples sizes. As DECT becomes more widely used clinically and more scientific studies evaluating the performance of DECT are published, DECT may eventually become an important modality in the work-up of infiltrative skeletal lesions. It may even challenge MRI and nuclear medicine because of relatively faster scanning times and ease of access.

Keywords Dual energy CT · Spectral CT · Bony metastasis · Skeletal lesion · Osseous lesion · Multiple myeloma

Introduction

Computed tomography (CT) is widely available in most clinical settings and has a relatively fast scan time. Many patients with cancer undergo CT examination as part of their oncologic care, and it is an invaluable modality in disease staging. Conventional monoenergetic CT, however, lacks sensitivity in screening for skeletal lesions, especially in metastatic lesions that are largely confined to the marrow space [1, 2], masked by the more highly attenuating cortical and trabecular bone. A meta-analysis found CT to have lower sensitivity (72.9%) compared to magnetic resonance imaging (MRI) (90.6%), positron emission tomography (PET) with CT (89.7%), and technetium-99 bone scintigraphy (86%) in detecting skeletal metastasis [3]. However, bone scintigraphy, though highly sensitive, can suffer from lack of specificity [4]. MRI can be relatively time-consuming when compared to CT and is not suitable for patients with claustrophobia or MRI incompatible aneurysmal clips, pacemakers, and defibrillators. PET-CT is limited by its low resolution in defining the margins of osseous lesions [5].

Dual energy CT technology was first investigated in 1976, not long after the invention of CT [6]. Practical clinical use of DECT was not realized until 2006 [7]. Current clinical uses of DECT have become more widespread [8]. In musculoskeletal imaging, DECT is used in the evaluation of crystal arthropathy, detection of subtle fractures not discernible on conventional CT, and metallic artifact reduction [9]. DECT is however, not commonly used in the evaluation of infiltrative skeletal neoplasms and metastasis. This review

✉ Martin Toby Tan
martin.tan.unsw@gmail.com

Thomas Bernard Lloyd
Thomas.Lloyd@health.qld.gov.au

[1] Department of Diagnostic Radiology, Princess Alexandra Hospital, 199 Ipswich Road, Woolloongabba, Brisbane, QLD 4102, Australia

summarizes current knowledge and research findings on the potential clinical applications of DECT in the detection and characterization of malignant skeletal lesions.

Dual energy CT technology

Conventional monoenergetic CT utilizes a spectrum of X-ray photons centered around a single peak and exploits differences in the material attenuation coefficients to generate images. However, materials with different elemental compositions may have similar attenuation coefficients at a single energy peak. In DECT, additional attenuation information is gathered from more than one X-ray energy peak. This is used to determine the chemical composition of materials based on the different degrees of X-ray attenuation over an energy spectrum that is influenced by the atomic weights and electron densities [8]. A spectral plot of attenuation coefficients of iodine, bone, and water varying with X-ray energy is shown in Fig. 1. At 100 keV, bone and soluble iodine has similar attenuation coefficients. At 50 keV however, the attenuation coefficients differ significantly due to the difference in K-edges [8, 10]. DECT exploits differences in both attenuation coefficient and material composition to generate clinically useful images [11].

Studies to date that have used DECT in the evaluation of skeletal lesions have mostly used reconstructions in the form of virtual non-calcium (VNCa), water-hydroxyapatite (water-HAP) material decomposition, and iodine differentiation maps. In VNCa images, acquired spectral data identifies and replaces calcium with a virtual CT number as close to the expected CT number, without calcium contributing to the total linear attenuation [12]. This results in better definition of bone marrow structure [13]. Skeletal lesions associated with bone marrow edema can be delineated on VNCa imaging [14]. In water-HAP material decomposition maps, spectral information of water and hydroxyapatite is used to map areas of increased water concentration, while suppressing bone [15]. With iodine contrast-enhanced DECT, iodine density mapping is used to quantify iodine uptake in tissue [16].

Skeletal metastasis

Bone is the third most common site for metastasis in cancer patients, resulting in painful and debilitating sequelae [17]. Skeletal metastasis is associated with advanced stages of cancer and a generally poor prognosis [18, 19]. Detection of skeletal metastasis is therefore vital for clinicians to tailor appropriate treatment and prevent further complications such as pathologic fractures [20]. Skeletal metastasis can be osteolytic, osteoblastic, mixed, or within bone marrow [15, 20, 21]. Metastatic lesions that neither destroy bone nor produce osteoblastic changes are not easily detectable with conventional CT. These lesions, which mainly involve the bone marrow, account for almost a third of all skeletal metastasis [22–24]. In a retrospective study of 2000 cases of skeletal metastasis, 41 cases were not detectable on CT but found on PET [22]. Staging and/or management had been affected in 29 of these 41 cases because of positive PET findings.

At the time of writing, we have identified a small number of retrospective reviews, one animal and one phantom model study that have studied the utility of DECT in evaluating skeletal metastasis, mostly with small patient numbers. MRI, bone scintigraphy, and occasionally histopathology were used as gold standard comparisons. This section discusses results from these studies, and key findings are summarized in Table 1.

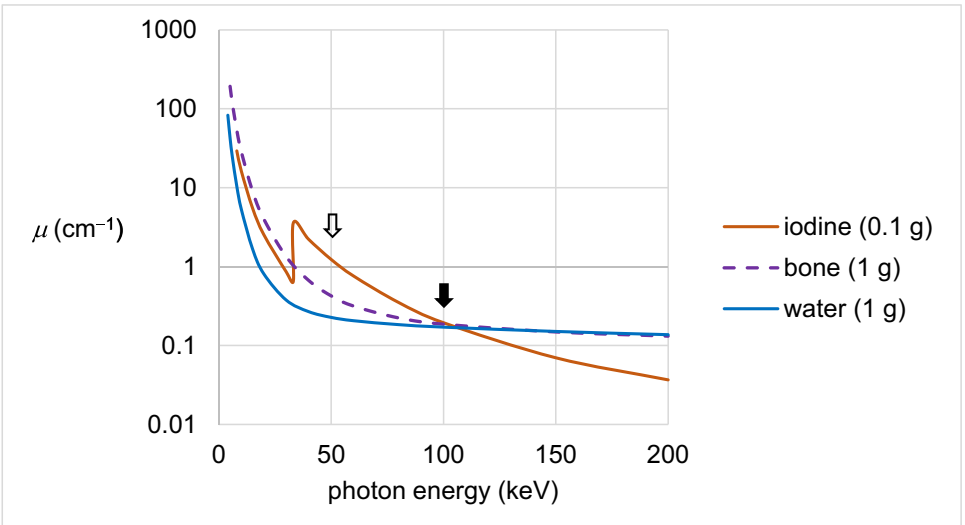

Fig. 1 Linear attenuation coefficient (μ) of bone, water, and of iodine, based on data from the National Institute of Standards and Technology [10]. At 50 keV, attenuation difference between iodine and bone is 0.8078 cm^{-1} (⇩). At 100 keV, this difference is 0.0087 cm^{-1} (⬇)

Table 1 Key findings from studies examining DECT in diagnosing metastatic skeletal lesions

Reconstructed images	Features
Virtual non-calcium (VNCa)	• Increased lesion attenuation on VNCa images [12, 25] • Color-coded bone marrow maps increased sensitivity of detection [25] • Low calcium suppression maps show improved sensitivity of detection compared to monoenergetic CT [12]
Iodine density map	• Increased iodine density in metastatic bone lesion compared to that in normal bone. With a threshold of iodine density of 4.5 mg mL^{-1}, sensitivity of detecting metastasis increased to 90.7% [16] • Steeper slope of the iodine density spectral curve in regions of soft tissue infiltration compared to soft tissue edema [5]
Hydroxyapatite-water decomposition images	• Improved sensitivity of detection compared to monoenergetic CT [15, 26] • Heterogeneous increase of water concentration in sclerotic and mixed type cortical bone metastasis, and homogeneous increase in bone marrow metastasis [15]

Calcium suppression in DECT used to generate VNCa images had been used for detecting bone marrow edema in vertebral fractures [27]. Images with higher calcium suppression index were found to detect bone marrow edema in fractures better. In the setting of iodine contrast-enhanced DECT, reconstructed images using lower calcium suppression indices were found to be more sensitive for detecting skeletal metastasis, which appeared as more hyperattenuating compared to surrounding tissue in VNCa images. In a retrospective study consisting of 21 patients with MRI-confirmed vertebral metastasis, the detection accuracy of iodine contrast-enhanced multi-level VNCa images was compared to conventional monoenergetic CT [12]. Images were reconstructed with low, medium, and high calcium suppression index. Low and medium calcium suppressed images were found to be more discriminatory of metastatic versus normal bone, as compared to high calcium suppressed images and conventional imaging. The sensitivity of detecting skeletal metastasis on low calcium suppressed images was also better (85%) compared to monoenergetic CT (78%). The authors attributed this finding to the similar attenuation profiles of calcium and iodine. In image maps reconstructed with higher calcium suppression levels, iodine was suppressed as well, and this decreased the iodine enhancement of metastatic lesions. In another small retrospective study, color mapping of bone marrow improved sensitivity of detecting skeletal metastasis from 78.2% on conventional CT to 89.8% [25]. The authors emphasized the importance of correlation with monoenergetic CT images, as two solely cortical lesions in the study were missed on the bone marrow color map images. Figure 2a–c and Fig. 2e–g are DECT images from our institute obtained on a patient with small cell lung cancer. The images illustrate the appearances of a L1 pedicle metastatic lytic lesion compared to T10 degenerative end plate erosions. Color-coded VNCa overlay reconstructions are shown in Fig. 2c and Fig. 2g. PET-CT axial images

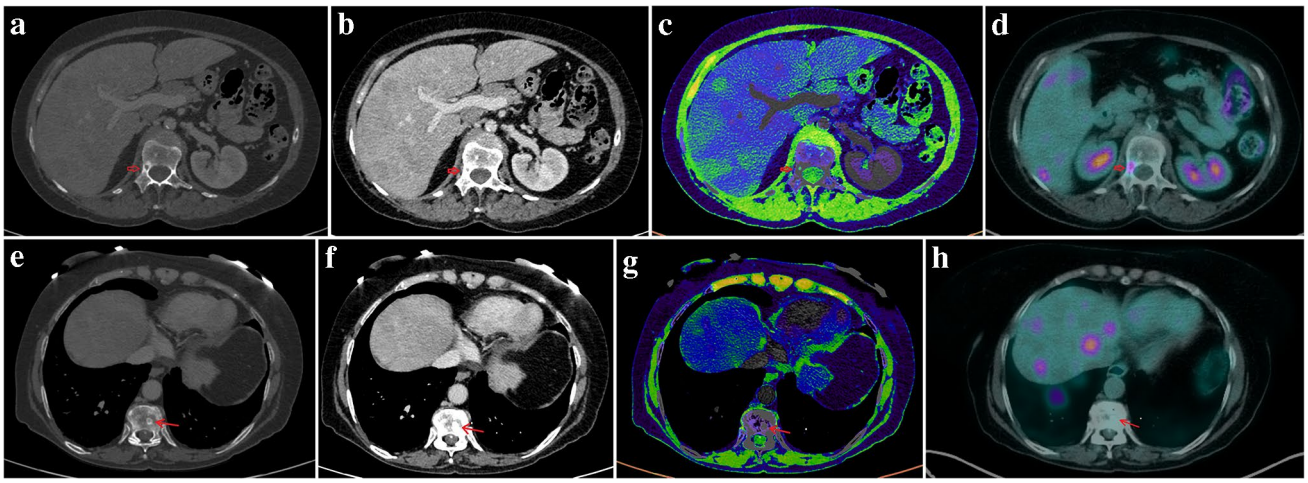

Fig. 2 Axial contrast-enhanced CT scan of a woman in her 60 s with small cell lung cancer metastasis. Right L1 pedicle metastasis (thick hollow arrow) in **a** bone window, **b** soft tissue window, and **c** color-coded VNCa overlay showing increased attenuation in the lesion (appearing green) and the **d** PET-CT performed 7 months earlier. Comparative appearance of a T10 vertebra degenerative end plate erosion (thin arrow) in the same patient in **e** bone window, **f** soft tissue window, and **g** color-coded VNCa overlay showing no increase in attenuation and the appearance on the earlier **h** PET-CT at the level of the T10 end plate erosion

obtained 7 months earlier at the level of the L1 pedicle metastasis and T10 degenerative endplate erosion are shown in Fig. 2d and Fig. 2h, respectively.

In iodine contrast-enhanced DECT, iodine maps and density quantification can be useful in detecting skeletal metastasis. In a retrospective review of 702 metastatic lesions on dual energy chest CT performed on 54 patients, bone-iodine spectral segmented images identified 92.3% of metastatic lesions that were initially confirmed on technetium-99 bone scintigraphy [28]. Quantification of iodine density may improve diagnostic accuracy further. In an animal study using rabbit models implanted with tumor fragments, iodine concentration was higher in areas of soft tissue infiltration compared to areas with soft tissue edema [5]. The authors were of the impression that tumor neovascularization and higher tissue permeability result in increased iodine contrast leakage. The slope of the attenuation spectral curve in regions of infiltrative lesions were greater compared to areas of normal tissue. Figure 3a–c are DECT images with iodine map reconstruction overlay from our institute obtained from the same patient in Fig. 2. A spectral plot comparing skeletal metastasis to normal bone is shown in Fig. 3d. PET-CT image obtained 7 months earlier at the level of the sternal lesion is shown in Fig. 3e. In a retrospective study of 43 consecutive cancer patients with vertebral bone metastasis compared to 40 cancer patients without bone metastasis, iodine density was found to be higher in infiltrated bone [16]. However, there was a significant overlap in the iodine density ranges in both infiltrated and healthy bone. Iodine density was also found to be reduced with increasing age and decreasing bone mineral density in the study. An iodine density threshold of more than 4.5–5.0 mg mL^{-1} was thought to be discriminative of infiltrated bone.

Water-hydroxyapatite imaging in non-contrast DECT may be useful in patients with iodine contrast allergies. Infiltrative skeletal lesions often show hyperintense T2 and hypointense T1 signals on MRI, due to the higher water content in tumor and replaced bone marrow compared to adjacent normal bone [26]. This same physical property change can be utilized on the water-HAP decomposition maps. In a study using lumbar spine phantoms embedded with simulated tumors (bone meal powder and magnesium-doped polyurethane rubber), a water-HAP material decomposition algorithm was more sensitive for detecting isoattenuating lesions compared to 70-keV virtual monoenergetic images (94% versus 82%) [26]. A more recent study evaluated the performance of water-HAP imaging in detecting skeletal metastasis in patients with prostate cancer [15]. Compared to normal bone, sclerotic and mixed type cortical bone metastases resulted in heterogeneous water density increases, and bone marrow metastasis resulted in a homogeneous water density increase. An example of a water-HAP image map from the study is shown in Fig. 4. Using water-HAP images to identify skeletal metastasis resulted in better diagnostic sensitivities and specificities (100% and 100%, respectively) compared to using 70-keV virtual monoenergetic images (74.2% and 71.0%, respectively).

Multiple myeloma

The International Myeloma Working Group (IMWG) recommends whole-body MRI in all patients with myeloma [29] as MRI can show infiltrative non-osteolytic lesions not easily visible on monoenergetic CT. DECT may become an important diagnostic and screening modality in multiple myeloma patients with contraindications to MRI. A handful of studies have evaluated the utility of DECT in detecting skeletal lesions and monitoring disease progression in multiple myeloma. These studies have examined using VNCa imaging on usually small patient sample sizes with MRI as the reference diagnostic gold standard. Table 2 summarizes key findings from the current studies.

Qualitative image analysis on VNCa images has been found to improve diagnostic yield compared to monoenergetic CT alone. Like skeletal metastasis, myeloma lesions appear hyperattenuating on VNCa images. A prospective study examined using VNCa images with color-coded overlay maps to identify bone marrow lesions [30]. The study comprised 34 patients with either multiple myeloma or monoclonal gammopathy of unknown significance (MGUS) who underwent DECT and MRI. There was improved sensitivity of detecting bone marrow lesions on VNCa color-coded overlay maps (91.3%) compared to standard monoenergetic CT imaging (69.6%). Another prospective study also found a higher sensitivity of detection on color-coded bone marrow VNCa images, but only for non-osteolytic bone marrow lesions (78.9%) compared to monoenergetic CT (24.8%) [33]. The difference in detection sensitivity was even greater for non-osteolytic diffuse infiltration patterns of disease, with sensitivities of 75% on VNCa imaging compared to 0% on monoenergetic CT. There was no difference in detection sensitivity between the two types of imaging for multifocal infiltration patterns. Figure 5a–c are non-contrast DECT images with color-coded VNCa overlay reconstruction obtained from a patient with multiple myeloma at our institute. Figure 5d is the axial diffusion weighted imaging (DWI) MRI showing the location of the myeloma deposit in the left posterior ilium.

More recent studies have utilized CT HU attenuation numbers to further characterize patterns of infiltrative skeletal lesions in multiple myeloma. In a group of 53 consecutive patients with known MGUS or multiple myeloma, the mean VNCa attenuation values were – 65.8 HU, 3.3 HU, and – 13.3 HU for normal bone, focal infiltration, and diffuse infiltration patterns, respectively [31]. The HU values

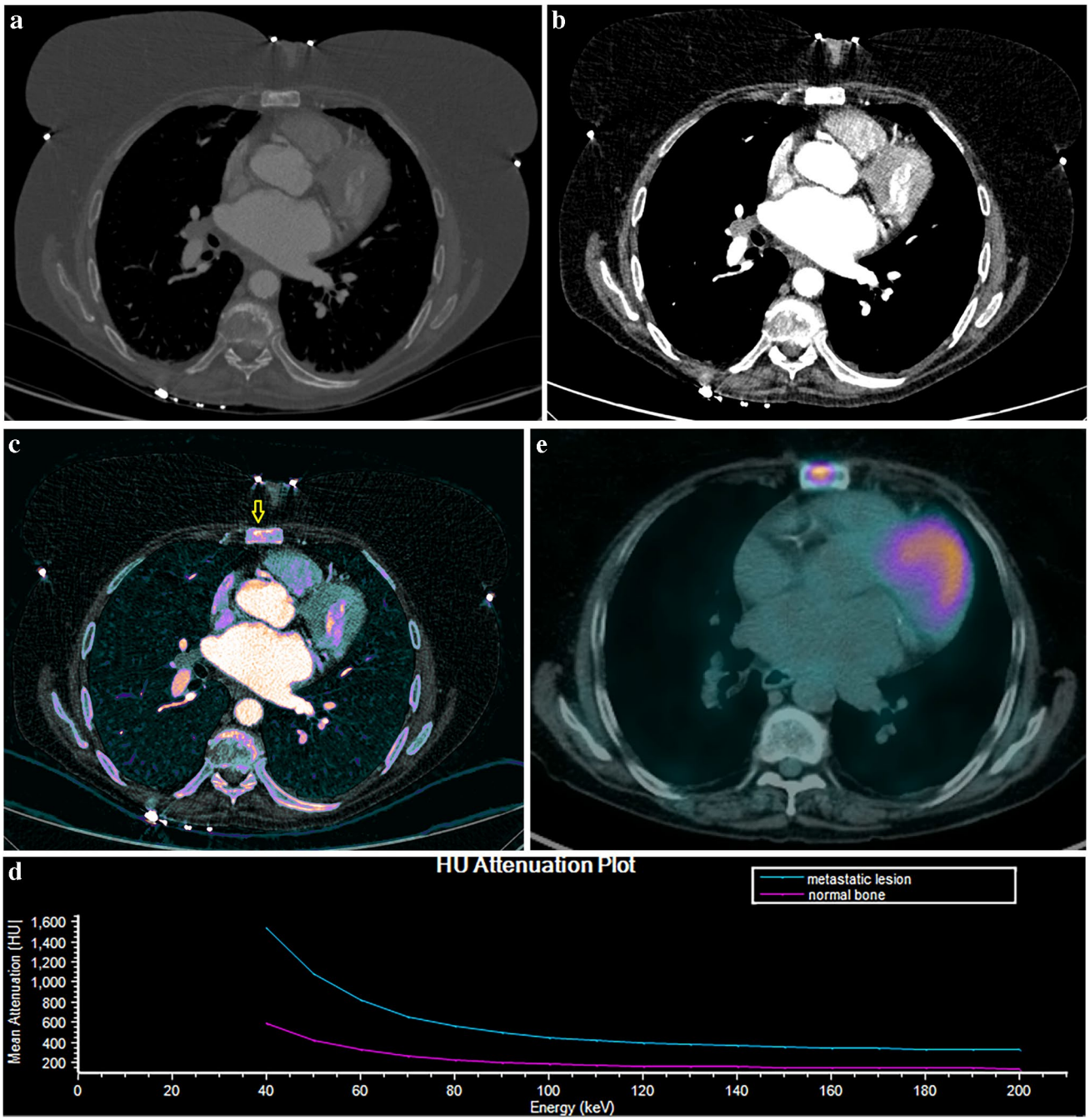

Fig. 3 Axial contrast-enhanced CT scan of a woman in her 60 s with small cell lung cancer metastasis to the sternum. **a** Equivocal findings for a metastatic in the sternum on virtual monoenergetic CT at 70 keV. **b** Image in soft tissue window. **c** Iodine-no-water maps reveals an increased focus of iodine uptake in the sternum (arrow). **d** Spectral plot of the metastatic lesion compared to normal bone. **e** Corresponding PET-CT showing the location of the sternal lesion

differed significantly between the normal versus infiltrated bone and in focal versus diffuse infiltrative patterns. Using a threshold of more than − 35.7 HU for identifying diffuse pattern lesions resulted in a detection sensitivity and specificity of 100% and 97%, respectively. There were similar findings in another prospective recruitment study, where regions over diffuse vertebral infiltrative lesions on VNCa imaging showed higher HU values compared to non-infiltrated vertebra [32]. A similar threshold value of more than − 37 HU was found to be 90.3% sensitive for detecting diffuse infiltrative lesions. An earlier prospective study, however, found higher mean VNCa HU values over areas of marrow invasion, with values of 4 HU and − 3 HU, respectively, for lytic and nonlytic lesions [33]. The differences in mean HU

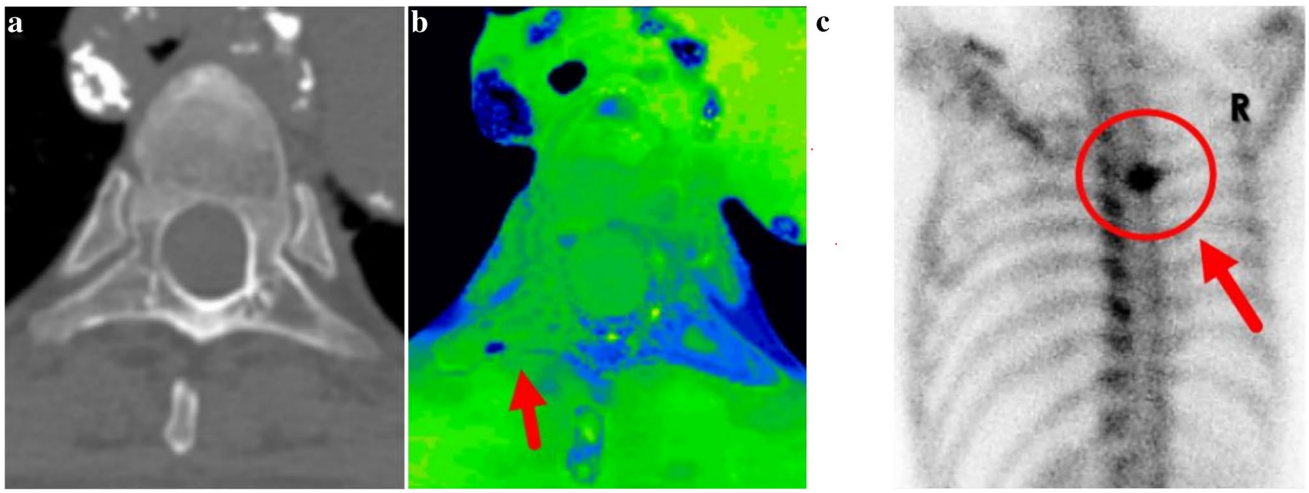

Fig. 4 A man in his 70 s with prostate cancer. **a** Axial conventional CT image shows no abnormal skeletal lesion in the T5 vertebra. **b** Increased water density in the right transverse process of T5 vertebra compared to the contralateral side in the water-HAP image. **c** Posterior view of bone scintigraphy showing metastasis to the right posterior element of the T5 vertebra. Reprinted from open access Creative Common CC BY license: MDPI Open Access Journals. Diagnostics (Basel). Improved Diagnostic Accuracy of Bone Metastasis Detection by Water-HAP Associated to Non-Contrast CT, Ishiwata et al. [15]

Table 2 Key findings of the appearances of multiple myeloma skeletal lesions on DECT

Utility of VNCa imaging in multiple myeloma	Findings from studies so far
Detecting lesions	• Regions of infiltrative vertebral lesions had higher VNCa CT HU values compared to normal bone [30–32]. Using a cut-off of more than − 37 HU and − 44.9 HU, the sensitivities of detecting infiltrative lesions were 90.3% and 93.9%, respectively [30, 32] • Color-coded VNCa images improved sensitivity of detecting bone marrow involvement [30], with a higher sensitivity of detection for diffuse patterns of infiltration [33] • DECT could not distinguish between red marrow reactivation and lesions from multiple myeloma [13]
Differentiating patterns of infiltration	• Average attenuation values over regions of focal and diffuse patterns were 3.3 HU and − 13.3 HU, respectively, compared to − 65.8 HU in normal bone [31] • Using a threshold of more than − 35.7 to − 37 HU results in a higher sensitivity for differentiating diffuse infiltration versus normal bone [31, 32]
Determining stage of disease	• Mean VNCa HU difference between skeletal lesions and background bone marrow was higher in active (35 HU) versus inactive disease (16 HU) [34] • On VNCa images, mean CT HU values over lesions negatively correlated with MRI T1W intensity [32, 34] • Patients with infiltrated vertebral bone marrow that show more uniform tissue structure and higher CT attenuation on texture analysis correlated with increased medullary infiltration on histopathology and more advanced stages of disease [35]

values found in these various studies were most likely due to different scan technologies and protocols.

Attenuation values on VNCa imaging correlates with disease activity in multiple myeloma. This may be useful for clinicians when monitoring treatment response. A recent retrospective study analyzed 103 axial skeletal focal osteolytic lesions in 32 patients [34]. The mean attenuation difference between regions of osteolytic lesions and surrounding normal bone marrow was determined on VNCa imaging and found to be higher in active disease (35 HU) compared to inactive disease (16 HU). Signal intensity on T1-weighted MRI is known to be useful in monitoring disease progression in myeloma patients. In two studies, VNCa HU values negatively correlated with T1-weighted MRI signal intensity [32, 34].

Texture analysis on VNCa imaging was found to correlate with disease burden in multiple myeloma. In a retrospective study of vertebral lesions in 110 patients who underwent whole-body DECT, texture analysis with a radiomics software was performed [35]. The texture analysis included examining "first-order features" that described the distribution of voxel intensities within the image region and

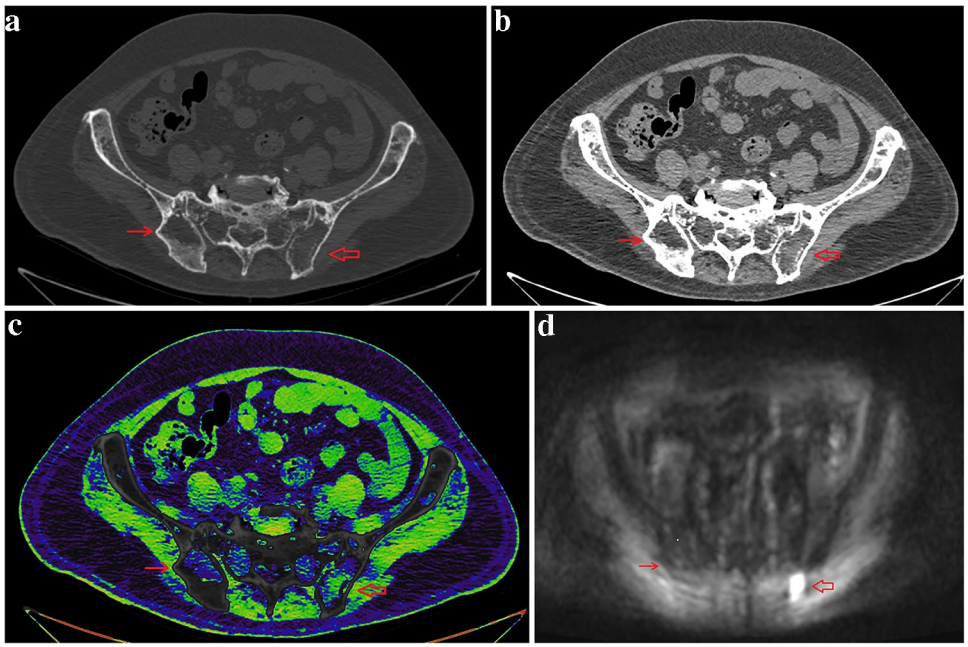

Fig. 5 Axial non-contrast DECT examination in a male patient in his 60 s with multiple myeloma in **a** bone window, **b** soft tissue window, and with **c** color-coded VNCa overlay showing the areas of myeloma deposit (thick hollow arrow) in the left posterior ilium which appears as an area of increased attenuation (green on the color-coded overlay), compared to an area of osteopenia (thin arrow, appearing mostly blue) in the right posterior ilium that was initially suspected to have myeloma deposits as well. **d** Axial DWI MRI with a *b* value of 800 s mm^{-2} obtained on the same patient shows myeloma deposits in the left posterior ilium, but not the right posterior ilium

"second-order features," also known as cluster prominence, which measured skewness and asymmetry of the gray-level co-occurrence matrix. Patients with more advanced stages of disease had higher first-order features and lower second-order features. Other first- and second-order subfeatures also correlated with serum-free light chains (SFLC), kappa/lambda SFLC ratio, and bone marrow myeloma infiltration on histopathology. The researchers concluded that multiple myeloma patients with infiltrated vertebral bone marrow that showed more uniform tissue structure and had higher CT attenuation on VNCa texture analysis correlated with histologically proven increased medullary infiltration and more advanced stages of disease.

A potential limitation of utilizing VNCa maps in evaluating multiple myeloma is a consequence of the DECT algorithm for three-material decomposition of images into bone mineral, yellow marrow, and red marrow. Red marrow can be represented either by plasma cell infiltration or erythropoietic reactivation in patients with multiple myeloma [13]. Therefore, VNCa imaging cannot distinguish between neoplasms or reactivated red marrow and will work best when imaging bone containing mostly fatty marrow [36]. As such, false-positive detection of multiple myeloma lesions on DECT may be a significant limitation [30].

Pathologic versus non-pathologic fractures

Pathologic fractures are complications of infiltrative skeletal lesions and metastasis. These are associated with debilitating pain, high morbidity, and a 20–30% decreased survival [37, 38]. Hence timely diagnosis is crucial. However, differentiating between fracture hematoma and infiltrative osseous lesions on conventional CT can be challenging. Methods in treating pathologic versus non-pathologic fractures are different. Orthopedic surgeons will often require CT in the work-up of pathologic fractures, as they provide valuable anatomic information for surgical planning. CT is also useful for determining the presence of other adjacent metastatic lesions which can interfere with the placement of internal fixation. In the after-hours setting, CT tends to be more easily accessible compared to MRI.

Features on conventional CT such as endosteal scalloping, periosteal reaction, soft tissue masses, and transverse fracture lines are reportedly useful in differentiating non-pathologic and pathologic fractures [39–41]. The presence of these features on conventional monoenergetic CT range greatly from 36 to 84% and suffer from poor interobserver agreement [42]. In a small retrospective review, colored bone marrow maps on DECT were used to analyze characteristics of 15 pathologic fractures in 11 patients [43]. Pathologic fractures had significantly higher HU attenuation values on the bone marrow maps compared to non-pathologic fractures (4.89 versus – 286.2). This difference was not observed on the virtual monoenergetic CT images. There have been no further studies that have evaluated this HU attenuation difference, and therefore, no known cut-off HU value on VNCa image maps that is known to differentiate between pathologic and non-pathologic fractures. It is therefore unknown if VNCa image maps on DECT can be clinically useful for this purpose. Further studies with larger numbers will be needed.

Differentiating malignant neoplasms from other benign lesions

Patients with cancer who are often elderly as well tend to undergo serial radiologic examinations as part of surveillance and/or assessing treatment response. Incidental findings when imaging elderly patients are common. It can be challenging to differentiate malignant infiltrative lesions from benign skeletal lesions. Two retrospective studies have used water-bone–based decomposition images and spectral curve analysis on DECT to differentiate these lesions [44, 45].

Both Schmorl's node and osteolytic metastasis are characterized by low-attenuating vertebral lesions with sclerotic margins. However, the physiological processes behind the two lesions are different. Osteolytic metastasis destroys and replaces bone, and metastatic tissue has increased vascularity compared to normal tissue. Therefore, osteolytic metastasis decreases bone but increases water content [46]. In Schmorl's node, the nucleus pulposus protrudes through the vertebral end plate into the cancellous bone, gradually compressing bone, but not significantly reducing bone content [44]. Water content of Schmorl's node is higher compared to a normal vertebra, due to the presence of the water-rich nucleus pulposus [47]. In a retrospective study evaluating 110 vertebral lesions in 102 cancer patients who underwent DECT, water- and bone-based material decomposition images were used to evaluate differences between Schmorl's nodes and osteolytic metastases [44]. In both metastatic lesions and Schmorl's nodes, bone densities were lower and water densities higher compared to normal vertebrae. When metastatic lesions were compared with Schmorl's nodes however, water density was higher in metastatic lesions (1009.2 mg cm^{-3}) compared to that in Schmorl's nodes (892 mg cm^{-3}), and average bone density of metastatic lesions was lower (43.57 mg cm^{-3}) compared to that of Schmorl's nodes (174.6 mg cm^{-3}). The spectral characteristics of metastatic lesions and Schmorl's nodes were also different. In virtual monoenergetic images below 100 keV, the mean HU of Schmorl's nodes was higher compared to metastatic lytic lesions. The HU values at a lower energy range on virtual monoenergetic images proved to be most useful for differentiating the two lesions. Images reconstructed at 40 keV resulted in an average attenuation values of 83.49 HU over regions of skeletal metastasis, compared to 216.41 HU for Schmorl's nodes.

Osteoblastic metastatic lesions can be challenging to differentiate from bone islands (enostoses), as both appear as focal hyperdense lesions with clear margins on monoenergetic CT. Attenuation measurements may help distinguish between the two. Osteoblastic metastasis is favored when a lesion has attenuation value below 885 HU on conventional CT [48]. DECT may further characterize these lesions using material decomposition. In a retrospective study of 94 patients with osteoblastic pulmonary metastases, water- and bone-based decomposition images were used to characterize osteoblastic metastases and bone islands [45]. Compared to bone islands, osteoblastic lung metastases had lower bone densities and higher water densities. The spectral curve slope for osteoblastic metastasis was also steeper. The authors suggested underlying physiological processes as the reason for the differences in DECT characteristics. Osteoblastic metastasis destroys original bone, thus reducing bone but increasing water content. In contrast, a bone island comprises normal cortical bone within the cancellous vertebral body, hence containing more bone but less water content than osteoblastic metastasis.

DECT-guided biopsy

Bone lesion biopsy is usually performed under CT guidance. Lesion localization is more straightforward if the lesion appears as radiolucent or radiopaque in comparison to the surrounding bone. However, when the target lesion has the same attenuation profile as adjacent bone on conventional CT imaging, the procedural radiologist will have to use anatomic landmarks based on other imaging modalities such as bone scintigraphy, PET, or MRI to guide the biopsy needle to the appropriate position. DECT may be utilized to increase the conspicuity of the lesion during the procedure, thus potentially improving target localization and diagnostic yield and reducing the need for repeat sampling.

A technical report publication described using DECT in guiding bone biopsies on four patients [11]. Bone lesions were identified on MRI and/or PET but not easily seen on monoenergetic CT. DECT-guided biopsy was performed with the aid of VNCa images. Lesions were localized to regions of abnormal color-coding on the bone marrow VNCa images that corresponded with prior PET or MRI images. The authors reported beam-hardening artifacts from the needle but used the beam artifact to direct the needle trajectory (Fig. 6). Final VNCa images were obtained after sampling to confirm that the needle intersected the lesion of interest.

A more recent case report described the use of electron density maps in DECT-guided biopsy of an iliac wing lesion in a woman with breast cancer [49]. PET-CT and the VNCa images were found to overestimate the dimensions of the metastatic bone lesion. The biopsy took only 22 min. The physical principle underlying electron density mapping is based on the variation in Compton attenuation between different materials. Compton scatter is greatly influenced by

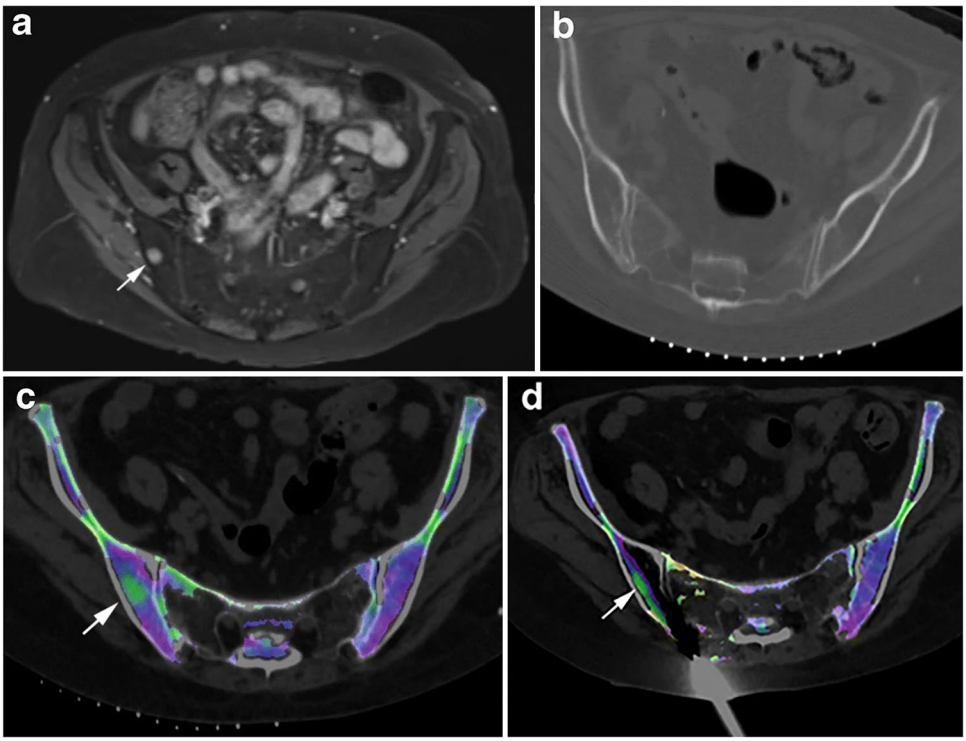

Fig. 6 Axial imaging of a patient with acute myeloid leukemia. **a** T1-weighted spin echo fat-suppressed post-contrast MRI shows an enhancing lesion in the posterior right iliac wing (arrow). **b** Axial CT from the initial biopsy does not show the target lesion, with no lesion cells identified at pathology. **c** Axial DECT with three-material decomposition algorithm for bone mineral, yellow marrow, and red marrow, fused with a VNCa color map overlay demonstrates the lesion. **d** Axial DECT color map with the needle on the surface of the posterior iliac wing directed toward the lesion shows beam-hardening artifact (arrow). The orientation of the artifact indicates the biopsy tract and can be helpful in directing needle advancement. The final pathology report yielded acute myeloid leukemia. Reprinted by permission from Springer Nature License and Copyright Clearance Center: Springer. Skeletal Radiology. Initial experience with dual-energy computed tomography-guided bone biopsies of bone lesions that are occult on monoenergetic CT, Burke et al. [11]

electron density, which in turn is determined by the composition of atoms and intermolecular bonds [50]. Metastatic lesions have higher cellularity compared to normal bone marrow. Consequently, metastatic lesions also have higher electron densities and attenuate X-rays by Compton scatter more than the photoelectric effect. Therefore, the higher cellular content on metastatic lesions compared to normal bone marrow can be exploited on electron density maps to delineate bone marrow lesions not easily apparent on monoenergetic CT.

A possible downside to performing DECT-guided biopsy might be the increased procedural time, due to additional image post-processing required to obtain optimal images for the procedure [51]. In the technical report of DECT-guided biopsies performed on four patients, the authors reported procedural time of more than 1 h for the first patient [11]. As the biopsy team became more comfortable with the technique and optimized imaging parameters, procedural times were reportedly only slightly greater than the usual bone biopsy times. Another issue to consider is radiation dose. Using DECT to perform image-guided biopsy may result in increased radiation dose delivery compared to using conventional CT. However, if less passes of the needle are needed, the overall dose from DECT-guided biopsy may be similar to, or possibly lower than, conventional CT-guided biopsy [51]. Further research with larger patient sample sizes will be needed to quantify the benefit and/or downsides of performing DECT-guided biopsies of skeletal lesions.

Future directions

DECT has brought about features not previously seen with monoenergetic CT. Photon counting detector technology will likely advance CT imaging even further. At the time of writing, the first photon counting dual energy CT device NAEOTOM Alpha (Siemens Healthineers) had just been approved by the US Food and Drug Administration through the premarket clearance pathway [52]. Potential benefits include higher resolution kernels, smaller noise grain sizes, as well as providing stable Hounsfield units in quantitative evaluation [53]. A recent case report evaluated

the performance of an experimental photon counting CT device in characterizing skeletal lesions of breast cancer patients [54]. Compared to images from conventional energy integrating detector CT, there was less inter-reader variability, and subjective improved visualization of lesion margins when reviewers analyzed images from the photon-counting detector CT. A combination of dual energy and photon counting technology may change the way skeletal lesions are visualized on CT in the future.

Conclusion

The role of CT in musculoskeletal imaging has diversified with dual energy technology. Currently, studies that have evaluated the performance of DECT in imaging malignant skeletal lesions have been mostly retrospective in nature, performed on small patient sample sizes. These studies have examined the utility of DECT in visualizing bone metastases, multiple myeloma lesions, pathologic fractures, and image-guided biopsies. There is currently no consensus on how skeletal lesions are characterized on DECT. Larger comparative studies and potentially evaluating the combination of photon counting and dual energy technology will be key to extracting the untapped potential of CT in musculoskeletal imaging.

Declarations

Ethics approval The Institutional Research Board had determined the review article to be compliant with the national ethical considerations in quality assurance and evaluation activities and waived the need for a human research ethics committee review.

Consent to participate Informed consent was obtained from the patients at our institute whose radiologic images are used in this review article.

Conflict of interest The authors declare no competing interests.

References

1. Yang P, Wu G, Chang X. Diagnostic accuracy of dual-energy computed tomography in bone marrow edema with vertebral compression fractures: a meta-analysis. Eur J Radiol. 2018;99:124–9.
2. Heindel W, Gübitz R, Vieth V, Weckesser M, Schober O, Schäfers M. The diagnostic imaging of bone metastases. Dtsch Arzteblatt Int Deutscher Arzte Verlag. 2014;111:741–7.
3. Yang H-L, Liu T, Wang X-M, Xu Y, Deng S-M. Diagnosis of bone metastases: a meta-analysis comparing ^{18}FDG PET, CT, MRI and bone scintigraphy. Eur Radiol. 2011;21:2604–17.
4. Palmedo H, Marx C, Ebert A, et al. Whole-body SPECT/CT for bone scintigraphy: diagnostic value and effect on patient management in oncological patients. Eur J Nucl Med Mol Imaging. 2014;41:59–67.
5. Chen H, Zhang Y, Pang J, et al. The differentiation of soft tissue infiltration and surrounding edema in an animal model of malignant bone tumor: evaluation by dual-energy CT. Technol Cancer Res Treat. 2019;18:1533033819846842. https://doi.org/10.1177/1533033819846842.
6. Alvarez RE, Macovski A. Energy-selective reconstructions in X-ray computerized tomography. Phys Med Biol. 1976;21:733–44.
7. Flohr TG, McCollough CH, Bruder H, et al. First performance evaluation of a dual-source CT (DSCT) system. Eur Radiol. 2006;16:256–68.
8. McCollough CH, Leng S, Yu L, Fletcher JG. Dual- and multi-energy CT: principles, technical approaches, and clinical applications. Radiology. 2015;276:637–53.
9. Mallinson PI, Coupal TM, McLaughlin PD, Nicolaou S, Munk PL, Ouellette HA. Dual-energy CT for the musculoskeletal system. Radiology. 2016;281:690–707.
10. Hubbell JH, Seltzer SM. X-ray mass attenuation coefficients. NIST Standard Reference Database 126 [Internet]. 2004 [cited 2021 Oct 31]. Available from: https://doi.org/10.18434/T4D01F
11. Burke MC, Garg A, Youngner JM, Deshmukh SD, Omar IM. Initial experience with dual-energy computed tomography-guided bone biopsies of bone lesions that are occult on monoenergetic CT. Skeletal Radiol. 2019;48:605–13.
12. Abdullayev N, Große Hokamp N, Lennartz S, Holz JA, Romman Z, Pahn G, et al. Improvements of diagnostic accuracy and visualization of vertebral metastasis using multi-level virtual non-calcium reconstructions from dual-layer spectral detector computed tomography. Eur Radiol. 2019;29:5941–9.
13. Palmer WE, Simeone FJ. Can dual-energy CT challenge MR imaging in the diagnosis of focal infiltrative bone marrow lesions? Radiology. 2018;286:214–6.
14. Chong CCW, Rai S, Nicolaou S. Dual energy CT in musculoskeletal tumors. In: De Cecco CN, Laghi A, Schoepf UJ, Meinel FG, editors. Dual energy in CT Oncology. Switzerland: Springer International Publishing; 2015. p. 147–52.
15. Ishiwata Y, Hieda Y, Kaki S, et al. Improved diagnostic accuracy of bone metastasis detection by water-HAP associated to non-contrast CT. Diagn Basel Switz. 2020;10:E853.
16. Borggrefe J, Neuhaus V-F, Le Blanc M, et al. Accuracy of iodine density thresholds for the separation of vertebral bone metastases from healthy-appearing trabecular bone in spectral detector computed tomography. Eur Radiol. 2019;29:3253–61.
17. Guillevin R, Vallee J-N, Lafitte F, Menuel C, Duverneuil N-M, Chiras J. Spine metastasis imaging: review of the literature. J Neuroradiol. 2007;34:311–21.
18. White AP, Kwon BK, Lindskog DM, Friedlaender GE, Grauer JN. Metastatic disease of the spine. J Am Acad Orthop Surg. 2006;14:587–98.
19. Roodman GD. Mechanisms of bone metastasis. N Engl J Med. 2004;350:1655–64.
20. Mundy GR. Metastasis to bone: causes, consequences and therapeutic opportunities. Nat Rev Cancer. 2002;2:584–93.
21. Gdowski AS, Ranjan A, Vishwanatha JK. Current concepts in bone metastasis, contemporary therapeutic strategies and ongoing clinical trials. J Exp Clin Cancer Res. 2017;36:108–108.
22. Ahmed F, Muzaffar R, Fernandes H, Tu Y, Albalooshi B, Osman MM. Skeletal metastasis as detected by 18F-FDG PET with negative CT of the PET/CT: frequency and impact on cancer staging and/or management. Front Oncol. 2016;6:208.
23. Yamaguchi T, Tamai K, Yamato M, Honma K, Ueda Y, Saotome K. Intertrabecular pattern of tumors metastatic to bone. Cancer. 1996;78:1388–94.
24. Suzuki A, Kashiwagi N, Doi H, Ishii K, Doi K, Kitano M, et al. Patterns of bone metastases from head and neck squamous cell carcinoma. Auris Nasus Larynx. 2020;47:262–7.

25. Issa G, Davis D, Mulligan ME. The ability of dual-energy computed tomography to distinguish normal bone marrow from metastases using bone marrow color Maps. J Comput Assist Tomogr. 2018;42:552–8.
26. Huang H-C, Srinivasan R, Sun Y, Kazakia GJ, Lin P-C, Yeh BM. Detection of lumbar spine osseous metastases using dual-energy CT: phantom results and preliminary clinical validation. Am J Roentgenol. 2019;212:402–10.
27. Neuhaus V, Lennartz S, Abdullayev N, et al. Bone marrow edema in traumatic vertebral compression fractures: diagnostic accuracy of dual-layer detector CT using calcium suppressed images. Eur J Radiol. 2018;105:216–20.
28. Lee YH, Kim S, Lim D, Suh J-S, Song H-T. Spectral parametric segmentation of contrast-enhanced dual-energy CT to detect bone metastasis: feasibility sensitivity study using whole-body bone scintigraphy. Acta Radiol. 2015;56:458–64.
29. Dimopoulos MA, Hillengass J, Usmani S, et al. Role of magnetic resonance imaging in the management of patients with multiple myeloma: a consensus statement. J Clin Oncol. 2015;33:657–64.
30. Kosmala A, Weng AM, Heidemeier A, et al. Multiple myeloma and dual-energy CT: diagnostic accuracy of virtual noncalcium technique for detection of bone marrow infiltration of the spine and pelvis. Radiology. 2018;286:205–13.
31. Kosmala A, Weng AM, Krauss B, Knop S, Bley TA, Petritsch B. Dual-energy CT of the bone marrow in multiple myeloma: diagnostic accuracy for quantitative differentiation of infiltration patterns. Eur Radiol. 2018;28:5083–90.
32. Wang Q, Sun Z, Li S, et al. Bone marrow imaging by third-generation dual-source dual-energy CT using virtual noncalcium technique for assessment of diffuse infiltrative lesions of multiple myeloma. Zhongguo Yi Xue Ke Xue Yuan Xue Bao. 2017;39:114–9.
33. Thomas C, Schabel C, Krauss B, et al. Dual-energy CT: virtual calcium subtraction for assessment of bone marrow involvement of the spine in multiple myeloma. Am J Roentgenol. 2015;204:W324–31.
34. Werner S, Krauss B, Horger M. Dual-energy CT-based bone marrow imaging in multiple myeloma: assessment of focal lesions in relation to disease status and MRI findings. Acad Radiol [Internet]. 2021 [cited 2021 Nov 29]; S1076-6332(21)00057-X. Epub 2021 Mar 8. Available from: https://doi.org/10.1016/j.acra.2021.01.029
35. Reinert CP, Krieg E, Esser M, Nikolaou K, Bösmüller H, Horger M. Role of computed tomography texture analysis using dual-energy-based bone marrow imaging for multiple myeloma characterization: comparison with histology and established serologic parameters. Eur Radiol. 2021;31:2357–67.
36. Rajiah P, Sundaram M, Subhas N. Dual-energy CT in musculoskeletal imaging: what is the role beyond gout? Am J Roentgenol. 2019;213:493–505.
37. Saad F, Lipton A, Cook R, Chen Y-M, Smith M, Coleman R. Pathologic fractures correlate with reduced survival in patients with malignant bone disease. Cancer. 2007;110:1860–7.
38. Behnke NK, Baker DK, Xu S, Niemeier TE, Watson SL, Ponce BA. Risk factors for same-admission mortality after pathologic fracture secondary to metastatic cancer. Support Care Cancer. 2017;25:513–21.
39. Bae JH, Lee IS, Song YS, et al. Bone tumors with an associated pathologic fracture: differentiation between benign and malignant status using radiologic findings. J Korean Radiol Soc. 2004;2015(73):240–8.
40. Fayad LM, Kawamoto S, Kamel IR, et al. Distinction of long bone stress fractures from pathologic fractures on cross-sectional imaging: how successful are we? Am J Roentgenol. 2005;185:915–24.
41. Mauch JT, Carr CM, Cloft H, Diehn FE. Review of the imaging features of benign osteoporotic and malignant vertebral compression fractures. Am J Neuroradiol. 2018;39:1584.
42. Fayad LM, Kamel IR, Kawamoto S, Bluemke DA, Frassica FJ, Fishman EK. Distinguishing stress fractures from pathologic fractures: a multimodality approach. Skeletal Radiol. 2005;34:245–59.
43. Issa G, Mulligan M. Dual energy CT can aid in the emergent differentiation of acute traumatic and pathologic fractures of the pelvis and long bones. Emerg Radiol. 2020;27:285–92.
44. Zheng S, Dong Y, Miao Y, et al. Differentiation of osteolytic metastases and Schmorl's nodes in cancer patients using dual-energy CT: advantage of spectral CT imaging. Eur J Radiol. 2014;83:1216–21.
45. Dong Y, Zheng S, Machida H, et al. Differential diagnosis of osteoblastic metastases from bone islands in patients with lung cancer by single-source dual-energy CT: advantages of spectral CT imaging. Eur J Radiol. 2015;84:901–7.
46. Jain RK. Determinants of tumor blood flow: a review. Cancer Res. 1988;48:2641–58.
47. Hauger O, Cotten A, Chateil J-F, Borg O, Moinard M, Diard F. Giant cystic Schmorl's nodes. Am J Roentgenol. 2001;176:969–72.
48. Ulano A, Bredella MA, Burke P, Chebib I, Simeone FJ, Huang AJ, et al. Distinguishing untreated osteoblastic metastases from enostoses using CT attenuation measurements. Am J Roentgenol. 2016;207:362–8.
49. Yamamoto S, Kamei S, Tomita K, et al. CT-guided bone biopsy using electron density maps from dual-energy CT. Radiol Case Rep. 2021;16:2343–6.
50. Huddleston AL, Sackler JP. The determination of electron density by the dual-energy Compton scatter method. Med Phys. 1985;12:13–9.
51. Dwijendra S, Burke M. Application of dual-energy computed tomography in bone lesion biopsy. Adv Clin Radiol. 2020;2:273–84.
52. U.S. Food and Drug Administration. FDA clears first major imaging device advancement for computed tomography in nearly a decade [Internet]. FDA; 2021 [updated 2021 Sep 30; cited 2021 Nov 28]. Available from: https://www.fda.gov/news-events/press-announcements/fda-clears-first-major-imaging-device-advancement-computed-tomography-nearly-decade
53. Siemens Healthineers. NAEOTOM Alpha with quantum technology [Internet]. Siemens; 2021 [cited 2021 Nov 28]. Available from: https://www.siemens-healthineers.com/computed-tomography/photon-counting-ct-scanner/naeotom-alpha
54. Wehrse E, Sawall S, Klein L, et al. Potential of ultra-high-resolution photon-counting CT of bone metastases: initial experiences in breast cancer patients. NPJ Breast Cancer. 2021;7:1–3.